Spectroscopic Studies of Boron Doped Titanium Dioxide Nanoparticles

Deependra D. Mulmi[1*], Dinesh Thapa[1,2], Biplav Dahal[1], Dinesh Baral[3], Pratima R. Solanki[4]

[1] Physical Science Laboratory, Faculty of Science, Nepal Academy of Science and Technology, Khumaltar, Lalitpur, GPO Box 3323, Nepal

[2] Department of Physics and Astronomy, Mississippi State University, Mississippi State, USA

[3] School of Physical Science, Jawaharlal Nehru University, New Delhi-110067, India

[4] Special Centre for Nanoscience, Jawaharlal Nehru University, New-Delhi-110067, India

* Corresponding author. Tel.: +977-9843-058819; email: dmulmi@gmail.com

Manuscript submitted June 3, 2016; accepted

doi: 10.17706/ijmse.2016.4.3.172-178

Abstract: Nano-sized Boron doped Titanium dioxide (B-TiO_2) particles were prepared by Sol gel method using Titanium isopropoxide, Boric acid and Deionized water in appropriate proportion. As-prepared samples were calcined at 500°C for 5 hours. The X-ray diffraction (XRD) results indicated that the synthesized nanoparticles have existed both in anatase and rutile phase. The size of B-TiO_2 nanoparticles was found 20.77 nm from the full width at half maximum of the XRD. The band gap energy of the boron-doped anatase nanoparticle was calculated 3.42 eV by the method of UV- Vis spectroscopy. The powder form of B-TiO_2 and Citric acid capped B-TiO_2 was analyzed through FTIR study. The Raman study of B-TiO_2 nanoparticles confirmed presence of mixture of the anatase and rutile phase.

Key words: Band gap, Nanoparticles, Raman spectra, UV-Vis spectroscopy

1. Introduction

Titanium dioxide (TiO_2) is one of the promising materials having numerous applications extending from common products (paints, cosmetics, toothpaste etc.) to the advanced technological applications such as photovoltaic cells, photocatalytic degradation of pollutants, water purification, bio-sensing and bactericidal action. TiO_2 is the most commonly used n-type semiconductors because of its high photo-catalytic activity and stability, relatively low cost and non-toxicity [1-4]. TiO_2 exists in three main crystalline forms: anatase, rutile and brookite. Rutile is the most thermodynamically stable phase whereas anatase and brookite are metastable phases. However, due to large surface area per unit mass and volume, anatase TiO_2 has greater photo-catalytic activity compared to rutile [5]. Anatase shows a band gap of 3.2 eV (a UV wavelength absorption of 385 nm). In contrast, rutile has a smaller band gap of 3.0 eV (in the visible light range 410 nm). Nevertheless, anatase is generally considered the most photochemically active phase of TiO_2. The reason for this higher activity is due to the combined effect of the higher surface adsorptive capacity of anatase and its higher rate of hole trapping. Recent studies have indicated that mixtures of anatase-rutile or brookite-anatase are more active than anatase alone [6-7]. Keeping these facts in mind, we have prepared TiO_2 nanoparticles with Boron doping. Here we report quite simple method of preparing B-TiO_2 nanoparticles and their characterization.

In recent years, a variety of synthesis methods such as hydrothermal method [8], solvothermal method

[9], sol-gel method [10], direct oxidation method [11], chemical vapor deposition (CVD) [12], electro-deposition [13], sonochemical method [14], and microwave method [15] have been used for the preparation of TiO_2 nanostructured materials. Herein, we employed simple, cost effective, and environmental benign sol-gel method for the synthesis of Boron doped TiO_2 nanoparticles. Boric acid was used as a source for Boron doping. The B-TiO_2 sample was characterized by X-ray diffraction, UV-Vis spectrophotometer, Fourier Transform Infrared spectrometer and Raman spectrophotometer.

2. Experimental

Chemicals used in this research work were of analytical reagent grade. They were utilized as obtained without any further refinement. All aqueous solutions were made using deionized water. For B-TiO_2 nanoparticles preparation, Titanium (IV) isopropoxide (TTIP) of Sigma-Aldrich was used as a starting material. The precursor was made by mixing TTIP, Boric acid and deionized water in the molar ratio of 1:10:200. The solution was stirred and dried at 80° C. The dried gel was grinded and calcined in a muffle furnace at 500° C for 5 hrs. And the dried crystals were transferred to a mortar and finally grinded to a fine powder which was used for further characterization. The procedure could be well understood from a simplified block diagram as shown in Fig 1. XRD analysis of the synthesized nanoparticle was carried out using CuKα radiation of D2 phaser Bruker at room temperature, ranging 2θ value from 20° to 65° with a scanning rate of 0.01° per second. UV–Vis spectra of B-doped TiO_2 were taken between 200 and 1100 nm by Cary 60 UV-Vis spectrophotometer (Agilent Technologies). Fourier transform infrared spectroscopy studies were performed from 400 to 4000 cm^{-1} with Varian FTS 7000 FTIR spectrometer. Raman spectra were recorded at room temperature with a Varian 7000 FT-Raman.

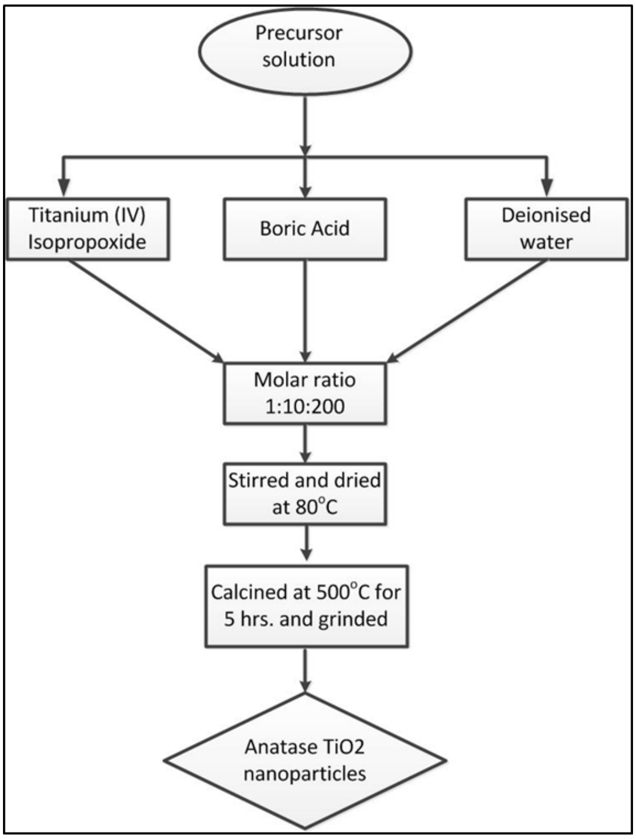

Fig. 1. Block diagram of experimental procedure to prepare boron doped TiO_2 by sol gel method.

3. Results and Discussions

3.1. XRD Analysis

The XRD pattern of the prepared boron doped TiO_2 measured at room temperature is shown in Fig. 2. Two strong peaks at $2\theta = 26.31^o$ and 28.96^o indicate the presence of anatase (101) and rutile (110) phases respectively. Other peaks at 38.80^o, 41.14^o, 48.97^o, 54.96^o, 55.98^o and 63.60^o can be attributed to (004), (112), (200), (105), (211) and (204) phases of anatase TiO_2 nanoparticles, respectively. The experimental XRD pattern agrees with the JCPDS card no 21-1272 for anatase and 21-1276 for rutile phase. Here, boron acts as an inhibitor for the growth of the anatase nanoparticles [16]. And more intense peak (110) is obtained for the rutile phase as shown in the Fig. 2. The average crystalline size of the boron doped TiO_2 nanoparticles is evaluated from the strongest diffraction peak at $2\theta = 26.31^o$ using Debye Scherer formula [17]

$$D = \frac{k\lambda}{\beta\, cos\theta} \tag{1}$$

Where k is the shape factor (0.9),
λ is the wavelength of CuKα radiation used (1.542 Å),
β is full width at half maximum,
θ is the angle of diffraction.

The calculated crystallite size for the anatase TiO_2 nanoparticles is 20.77 nm.

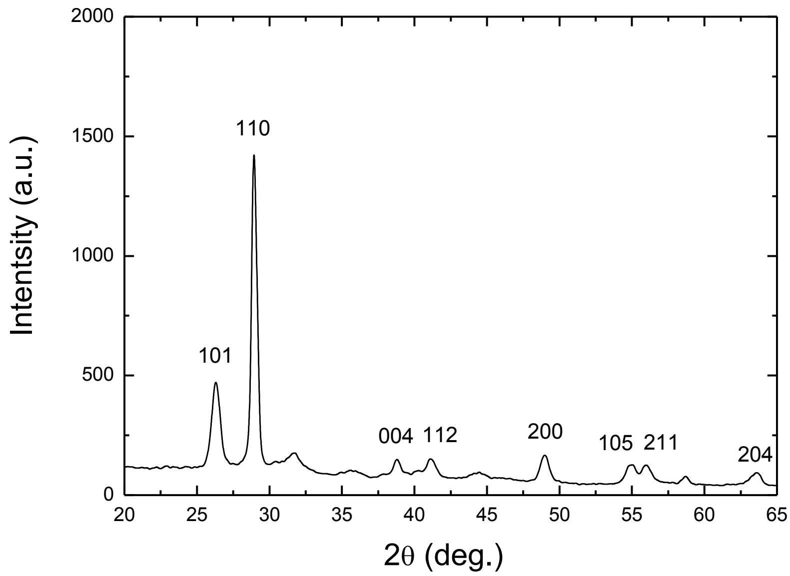

Fig. 2: XRD pattern of boron doped TiO_2 nanoparticles at room temperature.

3.2. UV-Vis Analysis

Fig. 3 shows optical absorption spectra of B-TiO_2 at room temperature. The absorption spectra exhibit strong absorption below 400 nm, corresponding to the intrinsic band gap of B-TiO_2 which is related to electron transitions from the valence band to conduction band. The direct band gap (E_g) of the samples is determined by fitting the absorption data to the direct transition equation [18]

$$\alpha h\upsilon = E_d \ (h\upsilon - E_g)^{1/2} \tag{2}$$

where α is the optical absorption coefficient,
$h\nu$ is the photon energy,
E_g is the direct band gap,
and E_d is a constant.

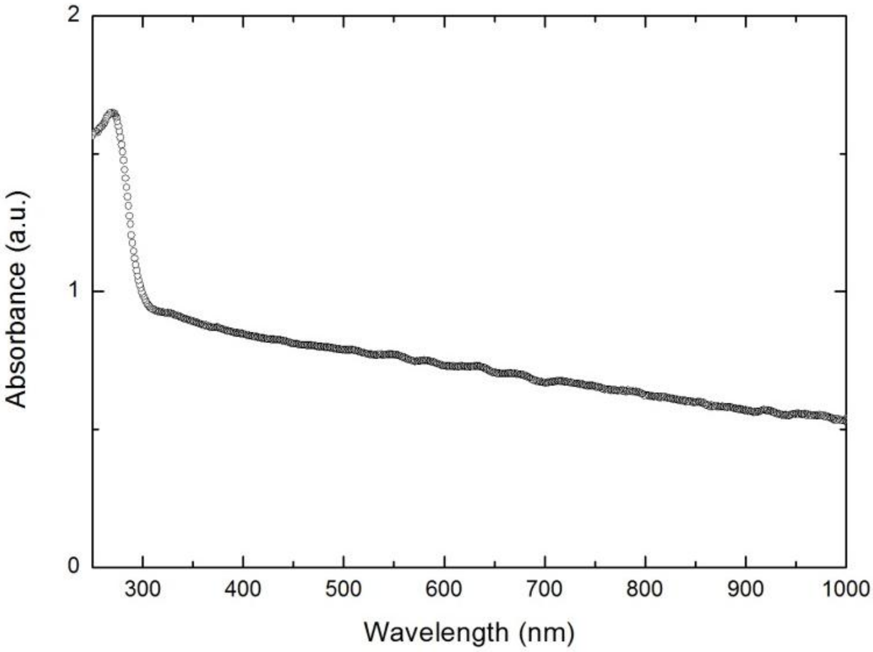

Fig. 3. The room temperature Optical absorption of B-TiO_2.

The band gap (E_g) is determined by extrapolating the linear portion of $(\alpha h\nu)^2$ versus $h\nu$ curve to $(\alpha h\nu)^2= 0$ in high absorption region as shown in Fig. 4. The band gap of B-TiO_2 is determined to be 3.42 eV.

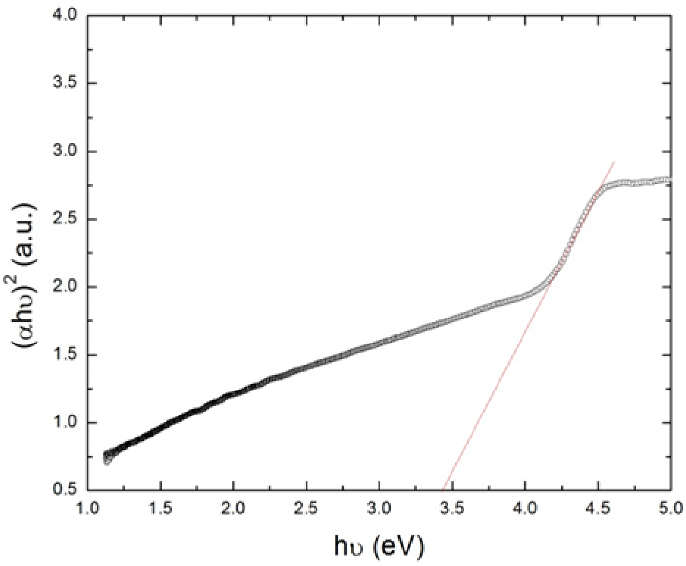

Fig. 4: Band gap energy of B-TiO_2 nanoparticles.

3.3. FTIR Analysis

The FT-IR spectra of the as prepared B-TiO_2 and Citric acid capped B-TiO_2 are shown in Fig. 5. The IR spectrum of B-TiO_2 shows main absorption peaks at 3950 cm^{-1}, 1800~ 2200 cm^{-1}, 991 cm^{-1} (solid line curve) [19-20]. The broad range of peaks from 1800~2200 cm^{-1} is assigned for bending vibrations of Ti-O. The new peak at 3950 cm^{-1} can be attributed to Boron doping on TiO_2. The shifting of peak from 1800~2200 cm^{-1} to 1000~1200 cm^{-1} suggested that there was a reaction of the carboxylic acid group with the surface of B-TiO_2. The peak around 1500 cm^{-1} is responsible for the carboxylate (COO-) stretching (dotted line curve) [21].

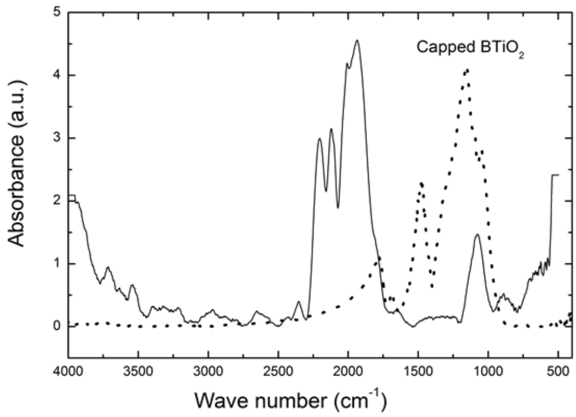

Fig. 5. FT-IR spectrum of B-TiO_2 (solid line) and citric acid capped B-TiO_2 (dotted line).

3.4. Raman Analysis

Raman spectroscopy is further employed to evaluate the structural properties of boron doped TiO_2 nanoparticles. Raman spectra (shown in Fig. 6) expresses Raman active modes at 145 cm^{-1} (E_g), 396 cm^{-1} (B_{1g}), 515 cm^{-1} (A_{1g}+B_{1g}) and 640 cm^{-1} (E_g), corresponding to anatase phase. Likewise, weak spectra of rutile phases are also observed E_g modes at 253 and 425 cm^{-1}. These absorption peaks are in good agreement with the results of TiO_2 [22]. New peak at 882 cm^{-1} suggests the bonding of Boron with TiO_2. E_g mode in Raman spectra is mainly caused by the symmetric stretching vibration of O-Ti-O bond, the B_{1g} mode is caused by the symmetric bending vibration of O-Ti-O, and the A_{1g} mode is caused by the anti-symmetric bending vibration of O-Ti-O [23].

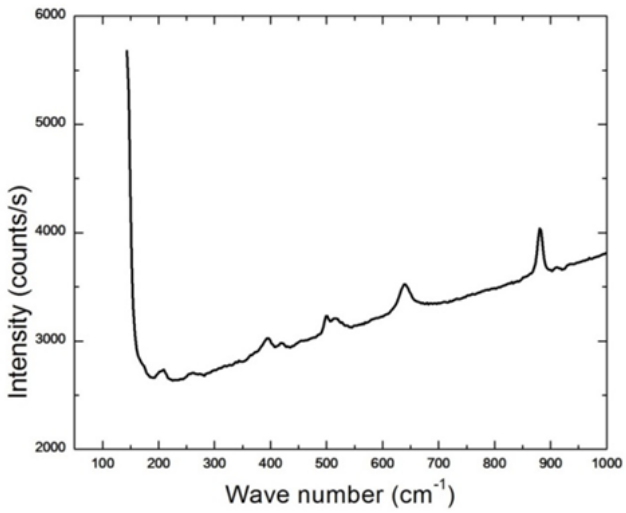

Fig. 6. Raman spectra of B-TiO_2 nanoparticles.

4. Conclusions

In the present work, nano-sized Boron doped Titanium dioxide was prepared by inexpensive Sol gel method. Samples were calcined at 500°C for 5 hours. From the X-ray diffraction, it was confirmed that the synthesized nanoparticles were found in both anatase and rutile phases. An average particle size of the resulting B-TiO_2 nanoparticles was found to be 20.77 nm computed from XRD analysis by using Debye Scherer's equation. The optical band gap energy was determined using absorbance spectra. The calculated band gap energy of B-TiO_2 nanoparticles were found to be 3.42 eV. The powder form of B-TiO_2 and Citric acid capped B-TiO_2 was analyzed through FTIR study. Main absorption peaks were observed at 3950 cm^{-1}, 1800~ 2200 cm^{-1}, 991 cm^{-1}. The broad range of peaks from 1800~2200 cm^{-1} were assigned for bending vibrations of Ti-O. The new peak at 3950 cm^{-1} could be attributed to Boron doping on TiO_2. The shifting of peak from 1800~2200 cm^{-1} to 1000~1200 cm^{-1} suggested that there was a reaction of the carboxylic acid group with the surface of B-TiO_2. It could be a sign of biocompatibility. The peak around 1500 cm^{-1} was responsible for the carboxylate (COO-) stretching. The Raman spectroscopy study had further supported presence of rutile and anatase phases. Raman spectra expressed Raman active modes at 145 cm^{-1}, 396 cm^{-1}, 515 cm^{-1} and 640 cm^{-1}, corresponding to anatase phase. Similarly, weak spectra of rutile phases were also observed at 253 and 425 cm^{-1}. New peak at 882 cm^{-1} suggested the bonding of Boron with TiO_2.

Acknowledgment

The first author is indebted to the research grant (RGA no: 12-143 RG/PHYS_AS_I-UNESCO FR:3240271367) from the TWAS (the World Academy of Sciences for the advancement of science in developing countries) for financial support.

References

[1] Reddya, K. M., Manorama, S. V., & Reddy, A. R. (2003). Band gap studies on anatase titanium dioxide nanoparticles. *Materials Chemistry and Physics, 78 (1)*, 239–245.

[2] Yogeswaran, U. & Chen, S. M. (2008). A review on the electrochemical sensors and biosensors composed of nanowires as sensing material. *Sensors, 8 (1)*, 290–313.

[3] Huang, Z., Maness, P. C., Blake, D. M., Wolfrum, E. J., Smolinski, S. L., & Jacoby, W. A. (2000). Bactericidal mode of titanium dioxide photocatalysis. *Journal of Photochemistry and Photobiology A: Chemistry, 130(2-3)*, 163-170.

[4] Sobczynski, A., & Dobosz, A. (2001). Water purification by photocatlysis on semiconductors. *Polish journal of Environmental Studies, 10 (4)*, 195-205.

[5] Chaturvedi, S., Dave, P. N., & Shah, N. K. (2012). Applications of nano-catalyst in new era. *Journal of Saudi Chemical Society, 16 (3),* 307–325.

[6] Shah, R. R., Kaewgun, S., Lee, B. I., & Tzeng, T. R. J. (2008). The antibacterial effects of biphasic brookite-anatase titanium dioxide nanoparticles on multiple-drug-resistant staphylococcus aureus. *Journal of Biomedical Nanotechnology, 4 (3),* 339-348.

[7] Miyagi, T., Kamei, M., Mitsuhashi, T., Ishigaki, T., & Yamazaki, A. (2004). Charge separation at the rutile/anatase interface: a dominant factor of photocatalytic activity. *Chemical Physics Letters, 390 (4-6)*, 399-402.

[8] Andersson, M., Österlund, L., Ljungstroem, S., & Palmqvist, A. (2002). Preparation of nanosize anatase and rutile TiO_2 by hydrothermal treatment of microemulsions and their activity for photocatalytic wet oxidation of phenol. *The Journal of Physical Chemistry B, 106 (41),* 10674-10679.

[9] Wahi, R.K., Liu, Y., Falkner, J.C., & Colvin, V.L. (2006). Solvothermal synthesis and characterization of anatase TiO_2 nanocrystals with ultrahigh surface area. *Journal of Colloid and Interface Science, 302 (2),* 530-536.

[10] Bazargan, M.H., Byranvand, M. M., & Kharat, A. N. (2012). Preparation and characterization of low temperature sintering nanocrystalline TiO_2 prepared via the sol-gel method using titanium (IV) butoxide applicable to flexible dye sensitized solar cells. *International Journal of Material Research, 103 (3),* 347-351.

[11] Ryu, W. H., Park, C.J., & Kwon, H. S. (2008). Synthesis of highly ordered TiO_2 nanotube in malonic acid solution by anodization. *Journal of Nanoscience and Nanotechnology, 8 (10),* 5467-5470.

[12] Shinde, P.S., & Bhosale, C.H. (2008). Properties of chemical vapour deposited nanocrystalline TiO_2 thin films and their use in dye-sensitized solar cells. *Journal of Analytical and Applied Pyrolysis, 82 (1),* 83–88.

[13] Tan, W., Chen, J., Zhou, X., Zhang, J., Lin, Y., Li, X., & Xiao, X. (2009). Preparation of nanocrystalline TiO_2 thin film at low temperature and its application in dye-sensitized solar cell. *Journal of Solid State Electrochemistry, 13 (5),* 651-656.

[14] Arami, H., Mazloumi, M., Khalifehzadeh, R., & Sadrnezhaad, S.K. (2007). Sonochemical preparation of TiO_2 nanoparticles. *Materials Letters, 61 (23-24),* 4559–4561.

[15] Corradi, A. B., Bondioli, F., & Focher, B. (2005). Conventional and microwave-hydrothermal synthesis of TiO_2 nanopowders. *Journal of the American Ceramic Society, 88 (9),* 2639-2641.

[16] May-Lozano, M., Ramos-Reyes, G.M., López-Medina, R.., Martínez-Delgadillo, S.A., Flores-Moreno, J., & Hernández-Pérez, I. (2014). Effect of the amount of water in the synthesis of B-TiO_2: Orange II photo degradation. *International Journal of Photochemistry, 2014 (721216),* 1-8.

[17] Guneri, E., Gode, F., Ulutas, C., Kirmizigul, F., Altindemir, G., & Gumus, C. (2010). Properties of p-type SnS thin films prepared by chemical bath deposition. *Chalcogenide Letters, 7 (12),* 685-694.

[18] Sze, S. M., & Ng, K. K. (2007). *Physics of Semiconductor Devices*. Hoboken, New Jersey: John Wiley & Sons, Inc.

[19] Mura, S., Greppi, G., Marongiu, M. L., Roggero, P. P., Ravindranath, S. P., Mauer, L. J., Schibeci, N., Perria, F., Piccinini, M., Innocenzi, P., & Irudayaraj, J. (2012). FTIR nanobiosensors for Escherichia coli detection. *Beilstein Journal of Nanotechnology, 3*, 485–492.

[20] Sheibley, D. W., & Fowler, M. H. (1966). Infrared Spectra of various metal oxides in the region of 2 to 26 microns (NASA-TN-D-3750). Cleveland, Ohio: National Aeronautics and Space Administration, Lewis Research Center, N-67-12798.

[21] Sharma, A., Baral, D., Rawat, K., Solanki, P.R., & Bohidar, H.B. (2015). Biocompatible capped iron oxide nanoparticles for Vibrio cholerae detection. *Nanotechnology, 26 (175302),* 1-10.

[22] Bettinelli, M., Dallacasa, V., Falcomer, D., Fornasiero, P., Gombac, V., Montini, T., Roman`o, L., & Speghini, A. (2007). Photocatalytic activity of TiO_2 doped with boron and vanadium. *Journal of Hazardous Materials, 146,* 529-534.

[23] Yan, J., Wu, G., Guan, N., Li, L., Lib, Z., & Caob, X. (2013). Understanding the effect of surface/bulk defects on the photocatalytic activity of TiO_2: Anatase vs Rutile. *Physical Chemistry Chemical Physics, 15*, 10978-10988.